Journal of Materials Chemistry A

Accepted Manuscript

This article can be cited before page numbers have been issued, to do this please use: X. Li, L. Zongbao, X. Yang, L. Jia, Y. Q. Fu, B. Chi, J. Pu and J. Li, *J. Mater. Chem. A*, 2017, DOI: 10.1039/C6TA10233F.

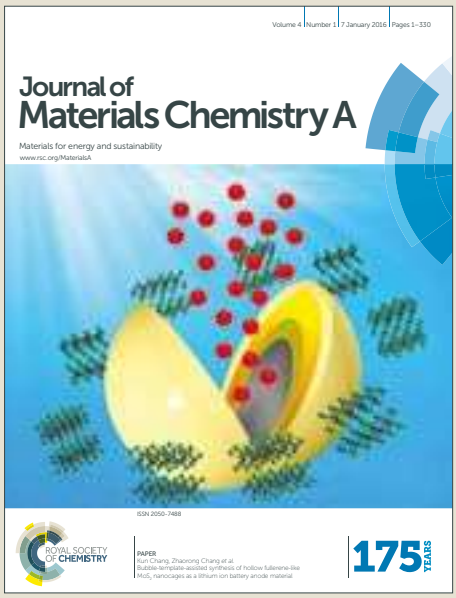

This is an Accepted Manuscript, which has been through the Royal Society of Chemistry peer review process and has been accepted for publication.

Accepted Manuscripts are published online shortly after acceptance, before technical editing, formatting and proof reading. Using this free service, authors can make their results available to the community, in citable form, before we publish the edited article. We will replace this Accepted Manuscript with the edited and formatted Advance Article as soon as it is available.

You can find more information about Accepted Manuscripts in the author guidelines.

Please note that technical editing may introduce minor changes to the text and/or graphics, which may alter content. The journal's standard Terms & Conditions and the ethical guidelines, outlined in our author and reviewer resource centre, still apply. In no event shall the Royal Society of Chemistry be held responsible for any errors or omissions in this Accepted Manuscript or any consequences arising from the use of any information it contains.

ROYAL SOCIETY OF CHEMISTRY

rsc.li/materials-a

View Article Online
DOI: 10.1039/C6TA10233F

Journal Name

ARTICLE

First-principles study of initial oxygen reduction reaction on stoichiometric and reduced CeO_2 (111) surfaces as cathode catalyst for lithium-oxygen batteries

Xinyu Li[a, b, d], Zongbao Li[c], Xiaofeng Yang [a], Lichao Jia*[a], Yong Qing Fu*[b], Bo Chi[a], Jian Pu[a], Jian Li[a]

CeO_2 has been explored as an electro-catalyst in the cathode of lithium-oxygen batteries due to its good performance, especially in the initial discharging stage. In order to fully understand its initial oxygen reduction reaction (ORR), in this work, oxygen and lithium adsorptions and initial ORR on the stoichiometric and reduced CeO_2 surfaces were systematically investigated using density functional theory (DFT) calculations. Changes of free energy values and structure parameters of the intermediates and precursors of the initial ORR were also studied to identify the possible reaction paths. It was found that the oxygen atoms are preferably adsorbed on the reduced CeO_2 surface, whereas the lithium atoms are preferably adsorbed on both stoichiometric and reduced CeO_2 surfaces, therefore, there exists a strong adsorption at the site with high oxygen coordinations. The reduced CeO_2 with the surface oxygen vacancies was identified as the most critical surface for the initial oxygen reduction reaction. The path with the lithium adsorption as the first step was identified as the most probable one. A Li_3O_2 precursor was identified as the most possible initial structure of the catalyst to start the discharging process.

Received 00th January 20xx,
Accepted 00th January 20xx

DOI: 10.1039/x0xx00000x

www.rsc.org/

Keyword: lithium-oxygen battery; oxygen reduction reaction; adsorption; first principles

1. Introduction

To cope with the significant greenhouse effect caused by the global emission of CO_2, a transition of key energy sources from fossil fuel to the electricity is urgently required, in which high energy density batteries play their critical roles. With their theoretically specific energy density comparable to that of gasoline, lithium-oxygen batteries (LOBs) have received extensive attention[1-4], although there are still many challenges to be solved, such as large overpotential and poor cyclability [5, 6].

To improve the electrochemical performance of the LOBs, different catalysts have been introduced into the oxygen cathode, such as metal oxides (MnO_2, Co_3O_4, and CeO_2) [7-10] , precious metals (Pt, Au and Ru) and their alloys[11-14], as well as metal carbides [15] . Among all these materials, ceria (CeO_2) is one of the promising catalysts due to its ability to catalyze both processes of oxygen reduction reaction (ORR) and oxygen evolution reaction (OER). Lin et al. [16] used CeO_2 as the cathode catalyst for the ORR in the LOBs and concluded that the crystal structure of the CeO_2 was critical to its electro-catalytic performance. Ahn et al.[10] reported that a relative high specific capacity can be achieved when graphene/doped ceria nano-blend was used as cathode catalyst a in the LOBs. Recently, our experimental study showed that the LOBs with a cathode of CeO_2 nanoparticles in-situ grown on nitrogen doped reduced graphene oxide (CeO_2@N-RGO) exhibited superior electro-catalytic activity and cyclability[17]. We also found that the presence of CeO_2 nanoparticles increased the capacity and cyclability of the LOBs. Besides, we found that there were 20.04% reduced Ce^{3+} in the CeO_2@N-RGO, and concluded that the remarkable catalytic activities of the CeO_2 in the LOBs were related to the oxygen vacancies on its surface [17].

Apart from its application in LOBs, CeO_2 is also considered as an active catalyst and widely used in automobile exhaust oxidation and solid oxide fuel cells (SOFCs), mainly due to its high oxygen ion conductivity. When it is used as the redox catalyst in the SOFCs, the easy shifting between the reduced and oxidized states provides enough three-phase reaction areas. With the development of the computational method and theories, first principles simulations are widely used to study

[a] Center for Fuel Cell Innovation, State Key Laboratory of Material Processing and Die & Mould Technology, School of Materials Science and Engineering, Huazhong University of Science & Technology, Wuhan, Hubei 430074, China. Email: jialc@hust.edu.cn
[b] Faculty of Engineering and Environment, University of Northumbria, Newcastle upon Tyne, NE1 8ST, UK. Email: richard.fu@northumbria.ac.uk
[c] School of Material and Chemical Engineering, Tongren University, Guizhou 554300, China.
[d] China-EU Institute for Clean and Renewable Energy, Huazhong University of Science and Technology, Wuhan, Hubei 430074, China.
† Electronic Supplementary Information (ESI) available:
See DOI: 10.1039/x0xx00000x

View Article Online
DOI: 10.1039/C6TA10233F

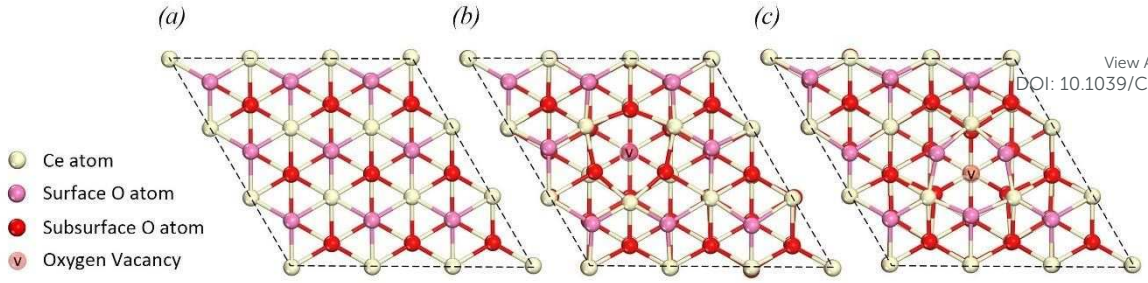

Fig. 1 Calculated stable structures of (a).ST (b).SOV and (c). SSOV CeO_2(111) surface.

the mechanism of catalytic reactions[18, 19].In order to fully understand the catalytic mechanisms of the CeO_2, many theoretical studies have been reported[20-22]. It is widely accepted that the oxidation proceeds on the CeO_2 surface mainly via a Mars-van Krevelen mechanism(redox mechanism), during which the reactant contacts with a surface oxygen atom to generate an oxidation product and an oxygen vacancy on the surface, followed by oxygen adsorption to fill the vacancy[23]. Using the first principles theory, Nolan et al.[20] found that the surface vacancies play a critical role for the conversion of CO, NO_2 and NO on the CeO_2 surface. By comparing the formation energies of H_2 and H_2O on both the stoichiometric and reduced CeO_2 surfaces, Wu[21] found that the H_2O reaction with a lower energy barrier occurs on the stoichiometric CeO_2 (111) surface. Theoretical analysis[22] proved that the ORR on the Ag/CeO_2 (111) surface preferably ended with the O_2 being reduced to O_2^{2-}.

To understand the mechanism and improve batteries' performance, many theoretical calculation works have also been conducted, such as the ORR and OER mechanism at different catalysts and aprotic solvent[24-28], prediction of possible product [29], and influence of electrolytes[30]. Although many studies have been carried out, there is no report as far as we know to investigate the mechanisms about lithium oxide reaction on the CeO_2 surface, including those related to lithium adsorption, formation and decomposition of lithium peroxide or other oxides. Moreover, there have been few studies about effects of stoichiometric and reduced CeO_2 on cathode reaction neither experimentally nor theoretically. Understanding the chemical processes occurring at the CeO_2 cathode is of great significance for the development of the LOBs.

In this paper, the adsorption of oxygen molecules and lithium atoms and different paths for initial ORR process on the CeO_2 (111) surface, which has been proved to be the most stable facet[31], were investigated using the density functional theory (DFT). Besides the stoichiometric (ST) CeO_2, surface oxygen vacancy (SOV) CeO_2 and subsurface oxygen vacancy (SSOV) CeO_2 were also investigated. The results obtained for reactions on CeO_2 (111) surface could be helpful to understand the processes on the other facets such as CeO_2 (100) or CeO_2 (110) surfaces.

2. Computational Details

The first-principles calculations were implemented in the Vienna ab initio simulation package (VASP) with a plane-wave basis set and a projector-augmented wave (PAW) method[32-34]. The electron-core interactions were represented by generalized gradient approximation (GGA) in the parametrization of Perdew-Burke-Ernzerhof (PBE) pseudopotential, and the cutoff of the plane-wave kinetic energy is 400 eV[35]. To solve the underestimate of the Ce (4f) states by the standard PBE, the DFT+U method was employed and the on-site Coulomb interaction correction with an effective U value of 5.0 eV was applied in the highly localized Ce-4f states[34, 36]. The examined lattice constant for bulk CeO_2 is 5.437 Å, agrees reasonably with the experimental value of 5.411 Å.[21]

A periodic slab with three CeO_2 atomic layers with *p*(3×3) lateral cells were used to construct the CeO_2 (111) surface, and a vacuum gap of 10 Å was introduced into the structure to prevent the interactions between slabs. The Brillouin-zone integration were sampled with 2×2×1 k-point mesh while the convergence criteria force was set to be 0.02 eV/Å for all surface calculations. All the atoms have been fully relaxed.

For the interstitial atoms absorbed on the surfaces, their adsorption energy (E_{ads}) is defined as:

$$E_{ads} = E_{tot} - E_{sub} - E_{Ori} \quad (1)$$

, E_{Ori} represent the total energies of adsorption configuration, substrate configuration (the ST, SOV or SSOV CeO_2 (111) surfaces) and original adsorbed species (Li or O_2 (*gas*)) respectively. The energy of a solvated Li^+ ion and one electron were set to be equal to bulk $Li_{(s)}$ as zero[37]. The total energy of O_2 includes the entropy of gas-phase O_2 at standard condition (298K)[38].

For the path of initial ORR, the change of the reaction free energy is defined as:

$$\Delta G_{(n)} = E_{tot_{(n)}} - E_{tot_{(n-1)}} - E_{Ori} \quad (2)$$

where $E_{tot_{(n)}}$, $E_{tot_{(n-1)}}$, E_{Ori}, represent the total energy of configuration at the *n* step, the total energy of configuration at *n-1* step, and the original energy of the adsorbed species (Li or O_2 (*gas*)).

To solve the problem of the well-known over-binding error of the energy of O_2 (*gas*) molecule, we employed the approach similar to ref [39] and calculated the formation energy values of bulk GeO_2, ZrO_2, SiO_2, and TiO_2, and obtained a corrected value of -0.81 eV for the binding energy.

3. Results and Discussion

3.1. Model verification

In this work, the lithium atom, oxygen adsorption and initial ORR process were calculated on both the stoichiometric and reduced CeO_2 (111) surfaces. Since the reduced CeO_2 (111) surface has been proven to have both surface and subsurface

View Article Online
DOI: 10.1039/C6TA10233F

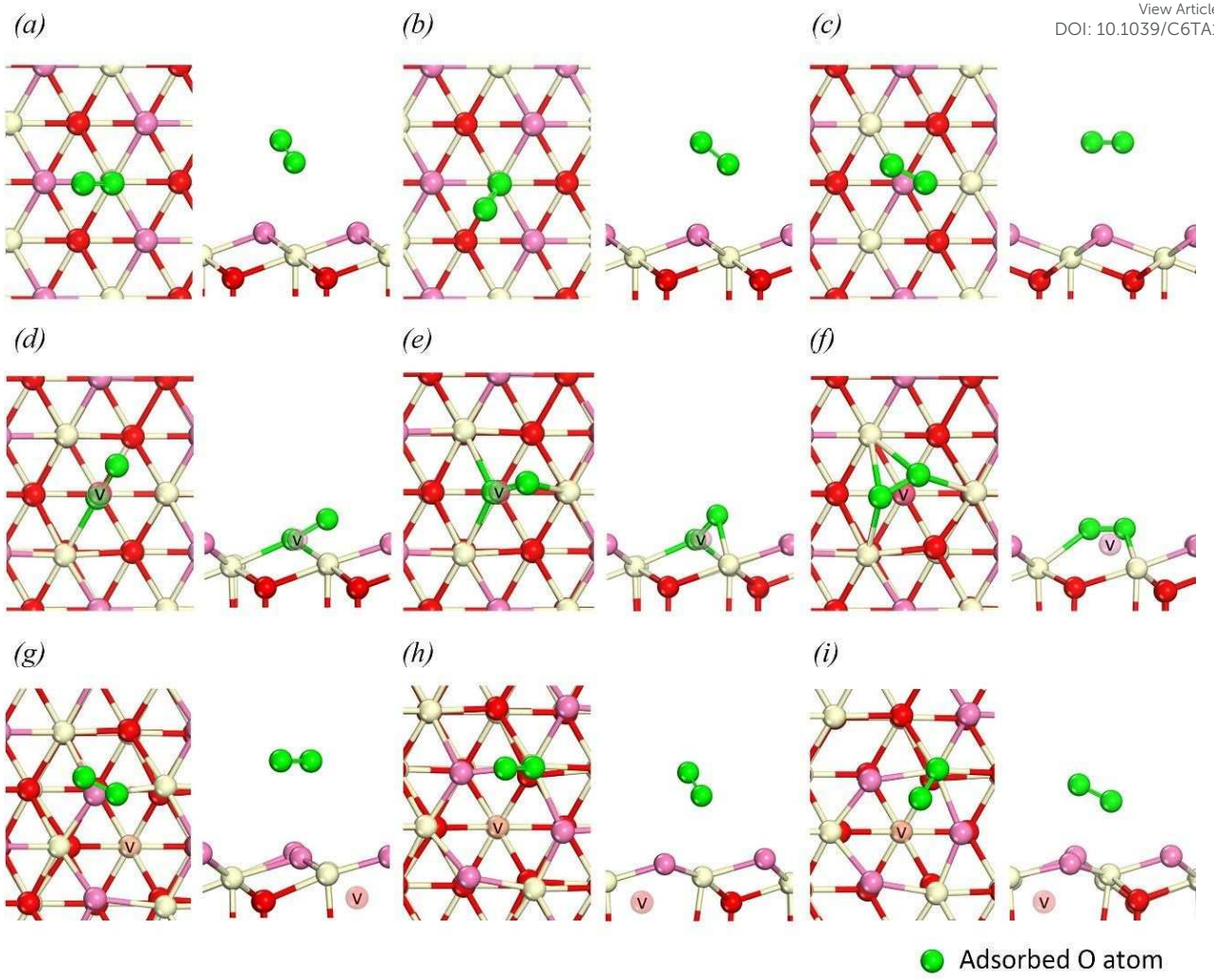

Fig. 2 Calculated structures (top view: left, side view: right) of oxygen species sites at ST CeO_2 (111) (a, b, c), SOV CeO_2(d, e, f), and SSOV CeO_2 (g, h, i).

oxygen vacancies[40], we took this into calculations, apart from the standard stoichiometric CeO_2 (111) surfaces (see Fig. 1). Results showed that on both the SOV and SSOV CeO_2 (111) surfaces, the obtained lowest formation energy structures (Fig. S1 and Table S1) are those with two excess electrons located at the next nearest Ce atoms, which is consistent with the literature[41].

3.2. Oxygen/lithium adsorption on the stoichiometric and reduced CeO_2 surfaces

The adsorption of oxygen molecule has been investigated because it is important at the beginning of discharge process in the LOBs. The optimized adsorption structures are shown in Fig. 2, and Table 1 summarizes the adsorption energies, geometrical parameters and partial charges for these configurations. Cases *a, b, c* are the oxygen molecules adsorbed onto the ST surfaces; cases *d, e, f* are those onto the SOV surface; while *g, h, i* are those onto the SSOV surface. From Fig. 2 and Table 1, we can conclude that: 1) the oxygen molecule adsorption on the ST and SSOV surfaces are physical adsorptions, with a weak adsorption energy and nearly zero charge transfer; 2) whereas on the SOV CeO_2 (111) surface, the O_2 molecule prefers to be adsorbed onto the vacancy site, with strong adsorption energies (-2.19, -2.17, -2.07 eV), long O-O bond and large charge transfer. The oxygen adsorption at the SOV CeO_2 (111) surface is most significant among all three surfaces, which is in a good

Table 1 Adsorption energies, geometrical parameters and charges (e) of adsorbed oxygen species on the ST, SOV and SSOV CeO_2 (111), which are corresponding to the configurations in Fig. 2.

Configuration	Energy(eV/O_2)	Adsorbed Height (Å)	d_{O-O} (Å)	Charges (e)
a	-0.22	2.51	1.23	0.03
b	-0.22	2.51	1.23	0.03
c	-0.21	3.30	1.23	0.02
d	-2.19	\	1.44	1.25
e	-2.17	\	1.45	1.21
f	-2.07	\	1.44	1.21
g	-0.18	3.22	1.24	0.04
h	-0.19	2.32	1.25	0.03
i	-0.14	1.90	1.27	0.02

View Article Online
DOI: 10.1039/C6TA10233F

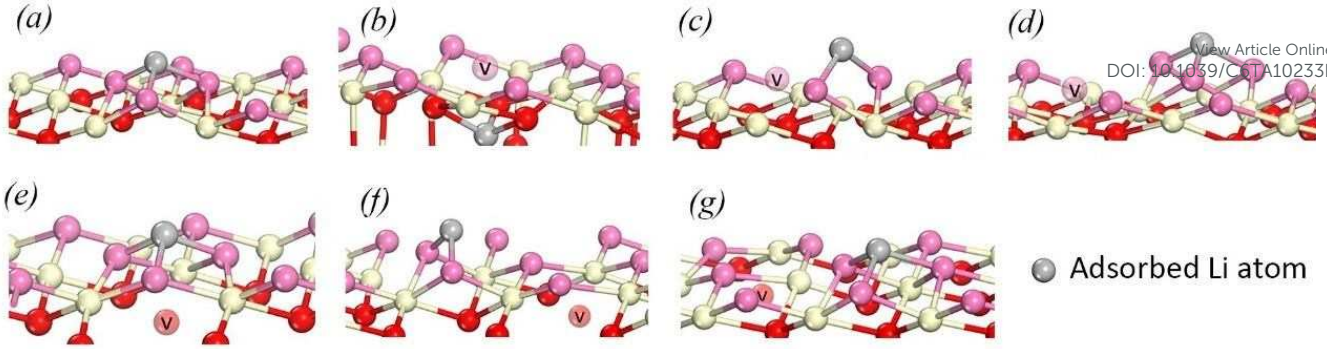

Fig. 3 Calculated structure of Li adatom sites at ST CeO_2 (a), SOV CeO_2(b, c, d) and SSOV CeO_2 (e, f, g)

agreement with the previous experimental and computational results [41-44] . Although both the SOV and SSOV configurations have Ce^{3+} ions on the surface, the existence of the SSOV did decrease the surface oxygen coverage, thus leading to a weak oxygen adsorption.

The optimized lithium adsorption structures are shown in Fig. 3, and the corresponding adsorption energies and structural parameters are summarized in Table 2. The detailed configurations and adsorption energies can be found in Fig. 2S and Table 2S. On the ST CeO_2 (111) surface, the adsorbed Li atom is bonded to the nearest three surface O atoms, with the lowest adsorption energy of -2.06 eV, thus leading to the increase of the distances between surface oxygen atoms and Ce atoms (2.77 Å, 2.81 and 2.89 Å compared to the initial 2.35 Å). It presents a strong adsorption behaviour for the high oxygen coordination, thus leading to the reduction of the Ce atom.

On the SOV surface, the 3-fold site has an adsorption energy of -1.78 eV. However, due to the long distance from the Li to the oxygen vacancy and the similar structural parameters, its adsorption behaviour is similar to that on the ST surface. Therefore, this was not taken into consideration in the following section. On the other hand, if the oxygen vacancy is filled with an oxygen atom, the Li adatom on the OB site will move to the 3-fold site. With a lower Li adsorption energy (-1.12 eV) compared to that of the hollow site (-0.99 eV), the most possible adsorption site of the Li is in the bridge of oxygen atom (OB) near the vacancy.

In the SSOV case, adsorption on the hollow up (HU) site has the most stable configuration, with the lowest adsorption energy of -2.25 eV. For the appearance of the subsurface O vacancy, the two next nearest Ce^{4+} ions are reduced to Ce^{3+} and their distances from the nearest O atoms are increased. Consequently, covalent electrons appear between the nearest surface O atoms and Li atom, leading to the higher adsorption energy. When the adsorption occurs on the OB site, the Li atom is located on the bridge of two next nearest O atoms through simulation, which is non-existed on the ST CeO_2 surface. In this case, the nearest O atoms move to the oxygen vacancy with the asymmetry and drive the Li atom to bond with two O atoms. However, in this case, the low coordination leads to a weak adsorption. For the adsorption on the 3-fold site, it was not taken into consideration in simulation due to the same reason as on the SOV surface, i.e., the long distance from Li to the oxygen vacancy and the similar structural parameters.

In order to obtain a clear picture about the charge transfer between the Li adatom and the surface, the Bader charge analysis[45] was performed. From the results listed in Table 2, it can be seen that the adsorbed Li atom contributes all the charge (+0.99 $|e|$ or +1.00 $|e|$) to the surface. Due to oxygen's -2 oxidation number, the charge should goes to Ce cations. However, the Bader charge analysis results (see Table 2) indicate there are only 0.22 ~ 0.29 $|e|$ charge goes onto the reduced Ce^{3+} cation. More effective evidence can be obtained by analyzing magnetic moments and density of states (DOS). Results showed that the reduced Ce^{3+} cations all have a magnetic moment of around 0.99 μ_B, which is consistent with Ce^{3+}'s magnetic moment reported in the published computational studies[46, 47].

To further understand the electronic properties of the Li adsorbed CeO_2 (111) surface, the total density of states (TDOS) and partial density of states (PDOS) for the most possible adsorption sites (3-fold on ST, OB on SOV, and HU on SSOV) were also calculated and the results are shown in Fig. 4. In the cases on the ST and SOV CeO_2 surfaces, the Li adsorption is accompanied by the appearance of a new Ce^{3+} peak in the DOS around the Fermi level. This new Ce^{3+} peak in the case of Li

Table 2 Adsorption energies surface and distances to the nearest surface oxygens (Li-O) of a Li adatom on the CeO_2 surface. The labels a-f correspond to the configurations in Fig.2.

	Site and Surface	Energy (eV/Li)	d_{Li-O} (Å)	d_{O-Ce} (Å)	Li donated Charges (e)	Ce^{3+} got Charges
a	3-fold on ST	-2.06	2.02,2.03, 2.06	2.77, 2.89, 2.81	-1.00	0.27
b	Hollow on SOV	-0.99	1.98, 1.98, 1.99	2.73, 2.74, 2.71	-1.00	0.26
c	OB on SOV	-1.12	1.90, 1.93	2.85, 2.99	-0.99	0.29
d	3-fold on SOV	-1.78	2.01, 2.02, 2.03	2.75, 2.84, 2.91	-1.00	0.22
e	HU on SSOV	-2.25	1.94, 1.94, 1.94	2.82, 2.82, 2.83	-1.00	0.27
f	OB on SSOV	-1.61	1.89, 1.92	2.77, 2.89	-1.00	0.27
g	3-fold on SSOV	-1.74	1.96, 2.04, 2.08	2.48, 2.53, 2.58	-1.00	0.24

View Article Online
DOI: 10.1039/C6TA10237F

adsorption on the SOV surface is due to special position of this Ce^{3+}', which has a shorter Li-Ce bond-length compared to the standard covalent length (2.80 Å vs. 2.88 Å). In the case on the SSOV CeO_2 surface, Li adsorption is accompanied with the increase of the Ce^{3+} peak. These results could further prove the reduction of the Ce atoms.

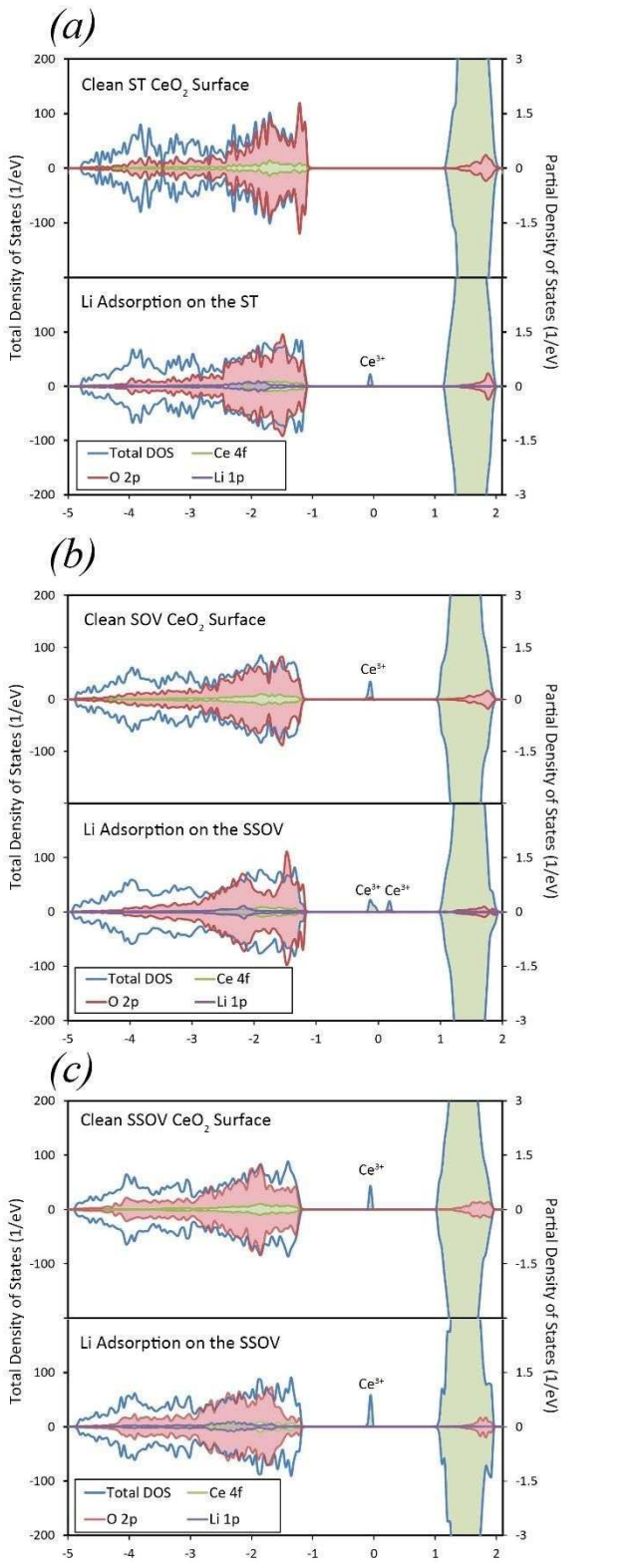

Fig. 4 The TDOS and PDOS of the clean and Li adsorbed ST(a), SOV(b), and SSOV(c) surfaces.

3.3. The Li_2O_2 precursors of initial ORR

Previously reported experimental results proved that the main discharge product in the cathode of an aprotic LOBs is Li_2O_2[48, 49], whereas it is Li_2O in some cases due to their similar formation energies (the formation energy is -2.86 eV for Li_2O compared to -2.90 eV for Li_2O_2)[50]. Considering the strong adsorption of Li atoms on the ST, SOV and SSOV CeO_2 (111) surfaces, two possible reaction paths can be listed as follows:

Path a: *Li → 2 *Li → $*Li_2O_2$ (3)

Path b: *Li → $*LiO_2$ → $*Li_2O_2$ (4)

For the SOV CeO_2 (111) surface which has a strong oxygen molecule adsorption, an excess path *c* is also considered:

Path c: $*O_2$ → $*LiO_2$ → $*Li_2O_2$ (5)

where the * represents adsorption site.

In order to investigate the precursors through different paths on the surfaces, it's critical to know their energies and structure parameters. The calculated energetic profiles of initial ORR are listed in Fig. S3 and Table S3 in the *Supporting Information*. The precursors are plotted in Fig. 5 with the same order corresponding to the paths shown in Fig. S3. Results of formation energy (the sum of the reaction energy), oxygen adsorption energy, Li-O bond-length and O-O bond-length are summarized in Table 3.

Fig. 5 (*a*)-(*d*) represent the possible precursors on the ST CeO_2 (111) surface. Case *a* with the molecule adsorption of -4.47 eV is more stable than case *b* with the dissociated adsorption of -3.85 eV. Case *c* shows the most stable configuration on the ST surface with a reaction energy of -4.49 eV, which is mainly due to the second Li atom's exothermic adsorption. The oxygen molecule adsorption in case *a* is more exothermic than those in the other cases, indicating the preferable oxygen adsorption on the ST CeO_2 surface. It is observed that the bond length of O-O (1.28 Å) in the case *a* is only 0.05 Å longer than that of gas-phase O_2. Considering the same O_2 bond length and high O coordination for the lithium atom, the interaction of the adsorbed Li atoms and O_2 molecule is weak in this case. It is also noticed that the oxygen dissociation and adsorption at the ST CeO_2 surface lead to a short Li-O length (i.e., 1.85-1.99 Å for case *b, c, d* compared to 2.09 Å for case *a*). Besides, as shown in Fig. S3, in the path of configuration *d*, the last adsorbed Li atom leads to a lattice oxygen out of its original site, where a dissociated O atom has been filled. It is obviously that Mars-van Krevelen mechanism (explained in Introduction) occurs here.

Fig. 5 (*e*)-(*g*) represent the Li_2O_2 precursors at the SOV CeO_2 (111) surface, with similar reaction energies varied from -6.42 eV to -6.68 eV. Especially, results show that the oxygen adsorption releases more energy with more pre-adsorbed Li atoms on the SOV CeO_2 (111) surface (e.g., -4.03 eV for case *e*, -3.22 eV for case *f*), compared to that of the first oxygen adsorption (i.e., -2.19 eV for case *g*).

Fig. 5(*h)* presents three Li atoms adsorptions followed by oxygen adsorption with an adsorption energy of -7.94 eV. For these cases, the oxygen molecules are always prefer to fill the vacancies with the O-O bond length varied from 1.48 to 1.50 Å. Results also showed that Li_2O_2 species on SOV CeO_2 surface (cases *e*, *f, g*) are similar to *c* and *d*, while their formation energy (-6.42 to -6.68 eV) is much lower than those of case *c* (-4.49 eV) and case *d* (-3.86 eV). The exothermic oxygen adsorption at the SOV CeO_2 is mainly caused by the filling of one oxygen atom onto the vacancy site. Table 3 also shows that the changes in the different adsorption sequences (i.e., among cases *e, f, g*) do not cause apparent structural differences.

The Li_2O_2 species formed on the SSOV CeO_2 (111) surface are shown in Fig. 5 (*i*)-(*k*). Cases *i* and *j* (path a) present two Li atoms adsorptions followed by oxygen adsorption and dissociated oxygen adsorption, respectively. The reaction path of case *j* is path *b* in Fig. 5. It is observed that the formation energy of case *i* (-5.21 eV) is lower than that of case *j* (-3.97 eV). Case *k* shows a configuration with a high formation energy the SSOV CeO_2 surface since one oxygen atom is not bonded to the Li atom. The Mars-van Krevelen mechanism is also observed in case *i*, with a surface oxygen atom replaced by an adsorbed dissociated oxygen atom. It is noticed that the O-O bond length on the SSOV CeO_2 (111) surface is longer than that on the ST surface, mainly due to the reduced Ce^{3+} on the SSOV surface.

For the oxygen adsorption of path *a*, when one of the dissociated oxygen atom locates at the center of two Li atoms and breaks the symmetry, the adsorbed Li atom at the OB site will move to the 3-fold site, thus leading to the dissociation adsorption which could release more energy than the adsorption on the ST CeO_2. The Li-O length in case *i* is similar to those in the cases at ST and SOV CeO_2. Case *k* is about when only one oxygen is bonded to two Li atoms, the Li-O bond length is longer, which could be the reason for its lower formation energy.

Table 3 Formation energies, oxygen adsorption energies, and configuration parameters of Li_2O_2 on the stoichiometric and reduced CeO_2 (111) surface. The configurations are corresponding to Fig. 5

Configuration	Formation Energy(eV)	Adsorption energy(eV/O_2)	d_{Li-O} (Å)	d_{O-O} (Å)
a	-4.47	-0.49	2.09, 2.09	1.28
b	-3.85	0.13	1.85, 1.85	\
c	-4.49	0.07	1.87, 1.92, 1.99	\
d	-3.86	0.07	1.85, 1.87, 1.91	\
e	-6.68	-4.03	1.99, 1.99	1.48
f	-6.66	-3.22	1.98, 1.98	1.48
g	-6.42	-2.19	1.92, 1.96	1.49
h	-7.94	-3.90	2.14,2.21*2, 2.37*2, 2.47	1.50
i	-5.21	-1.27	1.91, 1.97	1.34
j	-3.97	-0.03	1.95, 1.92	\
k	-3.77	0.45	1.99, 2.01	\

3.4. Most possible path of initial ORR and its effect to the cathode reaction in LOBs

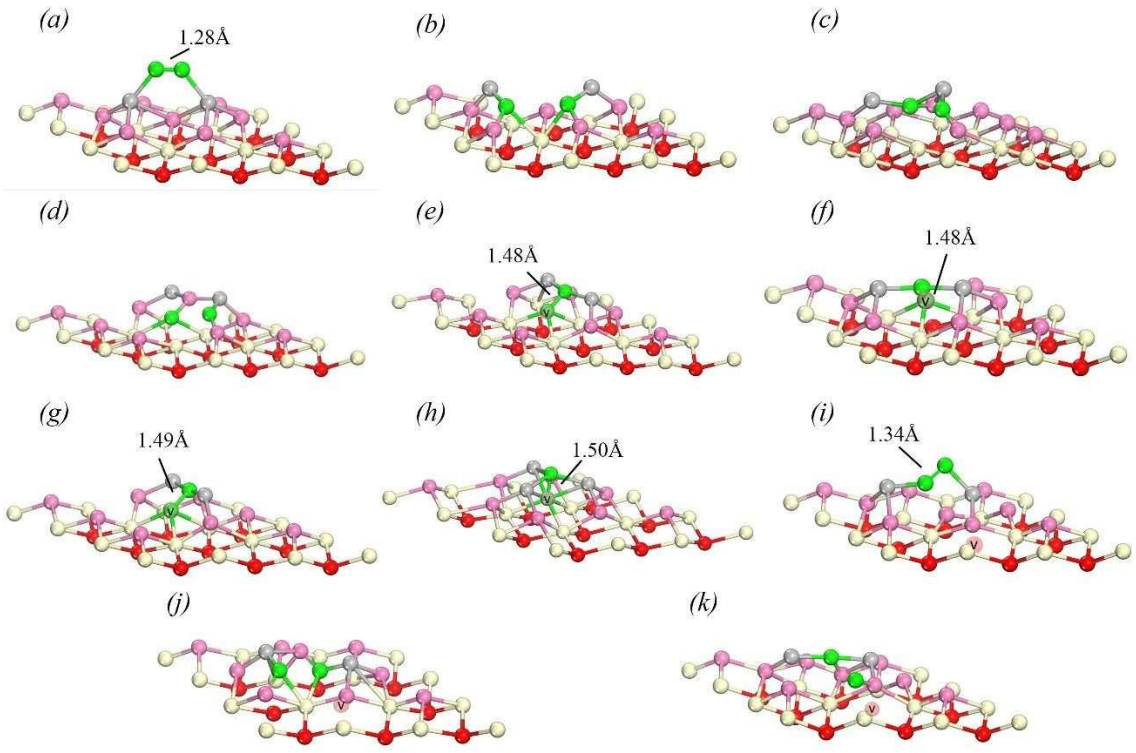

Fig. 5 Low energy initial ORR precursors at the ST, SOV and SSOV CeO_2 (111) surface. (a-d) precursors at ST CeO_2, (e-h), precursors at SOV CeO_2, (i-k) precursors at SSOV CeO_2.

Now we discuss the most possible reaction path and its influence to the cathode reaction in LOBs. First, the formation energies for bulk Li_2O_2 (-6.22 eV) and molecule Li_2O_2 (-2.93 eV) were calculated using same parameters, and then were compared with the Li_2O_2 initial reaction energy on the ST, SOV and SSOV CeO_2 (111) surfaces. Results showed that only on the SOV CeO_2 (111) surface there could be more energy released than that of the bulk Li_2O_2, and thus this would be the most possible surface for the initial ORR process. However, it is difficult to identify the reaction path simply from the energy and structure points of views, because all the paths lead to similar formation energies and structures (e.g., cases *e, f, g*). It is necessary to check the experimental process to understand the best path here. In most of the experimental battery preparation procedures, the electrolytes containing Li ions firstly contact the cathode[10, 17]. In the SOV CeO_2 cathode, surfaces with no, one, two or more Li atoms pre-adsorbed are co-existed. When the discharge process begins, the oxygen flows into the cathode and then is adsorbed on the surface. Among all the possible paths considered in this study, the adsorption of oxygen in path *a* releases the largest energy (see Fig. 6 *a*), indicating that path *a* is the most possible reaction path on the SOV CeO_2 (111) surface.

For most of the cases, the calculation of reaction through path *a* with two Li atoms and an oxygen molecule is reasonable[38, 51, 52]. However, in this work, adsorption of three Li atoms is also possible due to the structure symmetry, and the mechanism to form this situation is due to the existence of three OB sites for the Li adsorption on the SOV CeO_2 (111) surface as shown on Fig. 7. If there are only two Li atoms adsorbed on the surface, the initial ORR could happen through path *a*, as plotted in Fig. 7 *a, b, c.* In this case, one oxygen atom will occupy the vacancy site while the other oxygen atom tends to be adsorbed near the Li atom. However, if three Li atoms are adsorbed on the SOV surface, the reaction path can be defined as:

Path *d*: *Li →2 *Li →3 *Li → *Li_3O_2 (6)

The configurations through the path *d* have been plotted in Fig. 7 *a, b, e, f*, and their corresponding energy diagrams are plotted in Fig. 6 (b). The final Li_3O_2 precursor through path *d* has a special asymmetry configuration (Fig. 7 (d)), which has a similar formation energy (e.g., -6.59 eV, calculated by sum of 2/3*total lithium adsorption energy and oxygen adsorption energy) with the lowest formation energy of -6.68 eV. The precursor has structural parameters which are consistent with those of the O-rich Li_2O_2(0001)[53]. Hummelshøj et al.[53] systematically studied the over-potential of Li_2O_2 grown on different facets, and found that the O-rich Li_2O_2 (0001) leads almost zero over-potential for crystal growth at kinks, which could be interpreted as growth at the edge of this facet. Our result proves that the Li_3O_2 cluster can provide a suitable position for the Li_2O_2 crystal growth.

Based on the above discussion, we can conclude that the possible reactions at the CeO_2 cathode surface should be listed as follows. At the beginning of discharging, a lot of Li_2O_2 and Li_3O_2 clusters are generated through paths *a* and *d* on the SOV

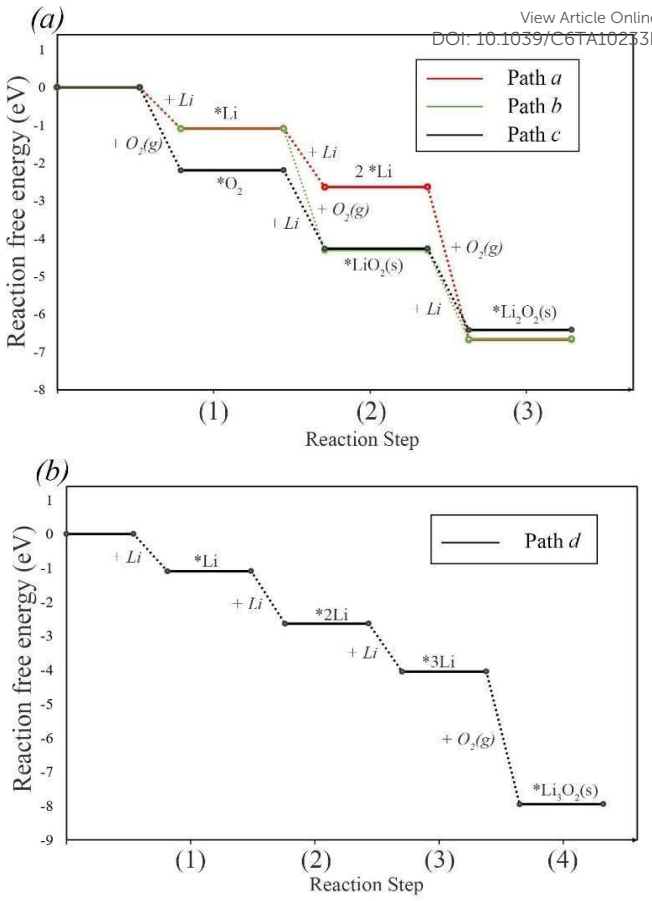

Fig. 6 Calculated energetic profiles of the initial ORR on the SOV CeO2 through paths a, b, c (a) and path d (b).

CeO_2 (111) surface. Due to the special structure of Li_3O_2 and conductive nature of the cathode, after all the surface vacancies have been filled by Li_2O_2 or Li_3O_2 clusters, the Li_2O_2 crystal prefers to grow on the top and edge of these clusters until all the cathode surfaces have been covered. This could explain the key reason that the main product in the CeO_2 cathode is still the Li_2O_2. Similarly, the same formation energy of -5.21 eV was predicted for the growth of Li_2O_2 clusters at the in-plane tetra-N pyridinic graphene, which has been proven to have the best electro-catalytic at the initial nucleation of Li_2O_2 [38]. This could also provide the evidence that the Li_2O_2 was firstly formed on the surfaces of CeO_2 nanoparticles, instead of on N-RGO[17] .

4. Conclusion

The redox behaviors of the stoichiometric and reduced CeO_2 surfaces have been investigated using first-principles method. The following conclusions can be made:

(1) Oxygen molecule is strongly adsorbed on the vacancy site of SOV CeO_2 (111) surface, whereas weak adsorptions are found on both the ST and SSOV surfaces. On the Li pre-adsorbed CeO_2 (111) surface, the oxygen molecular adsorption is more preferable than dissociative adsorption.

View Article Online
DOI: 10.1039/C6TA10233F

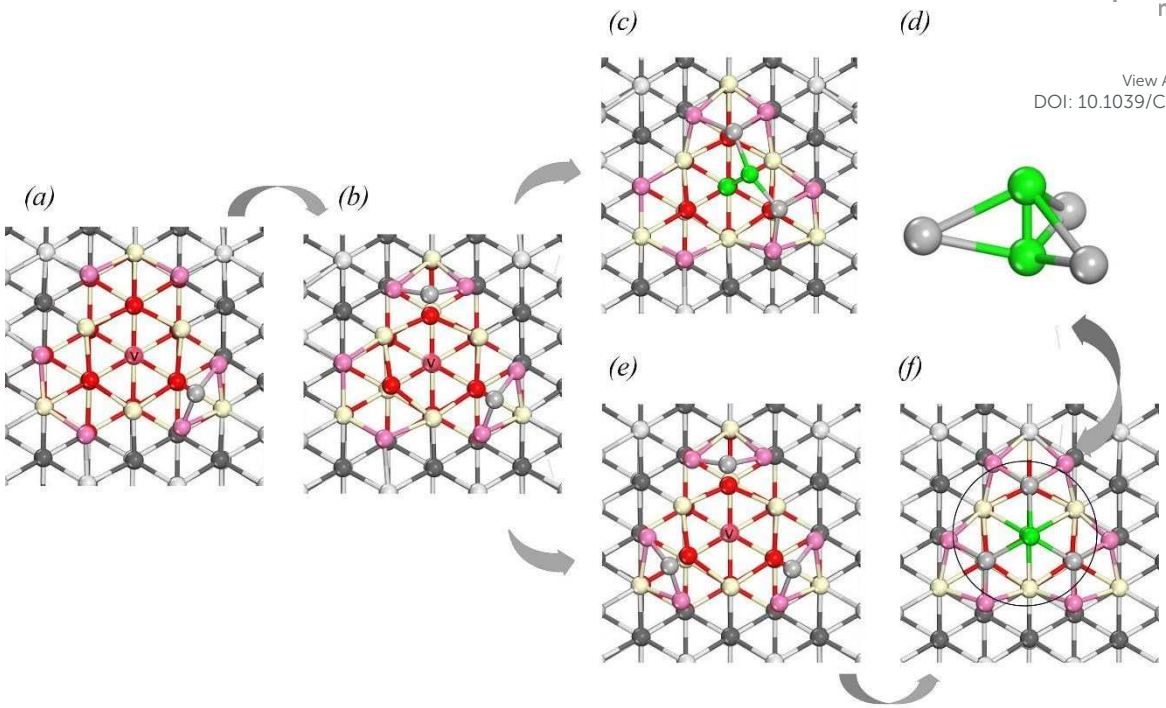

Fig. 7 Schematic for reaction path at the OB site. (a, b, c) Li_2O_2 precursor through path a on the SOV surface; (a, b, e, f) Li_3O_2 precursors through path d on the 1SOV surface (d) side view of Li_3O_2 precursor.

(2) Li atom is strongly exothermically adsorbed on the ST, SOV and SSOV CeO_2 (111) surfaces. Generally, the Li adatom obtained the strongest adsorption energy on the site which has the high oxygen coordination. The Li adsorption would also lead to a nearest or next-nearest Ce atom be reduced to Ce3+, and the charge transferred from the Li atom is randomly located to the coordinated O atom and the reduced Ce3+ atom.

(3) The initial ORR process calculation shows that the lithium oxide is energetically favorable on the SOV CeO_2 (111) surface, which means the decreased formation energy for the initial ORR. This good electro-catalytic ability is mainly due to the exothermic energy at oxygen adsorption, Li adsorption and Li oxidation.

(4) Among all the possible configurations at the SOV CeO_2 (111) surface, there is a Li_3O_2 cluster which has similar structure parameters with Li_2O_2 (0001) surface. This Li_3O_2 cluster provides a suitable position for the Li_2O_2 growth. It is concluded that this configuration on the SOV CeO_2 (111) surface plays the most important role at the initial ORR.

Acknowledgements

The authors would like to thank State Key Laboratory of Material Processing and Die & Mould Technology for computational assistance.

References:

1. P. G. Bruce, S. A. Freunberger, L. J. Hardwick and J. Tarascon, *Nat Mater*, 2012, **11**, 19-29.
2. J. Lu, L. Li, J. Park, Y. Sun, F. Wu and K. Amine, *Chem Rev*, 2014, **114**, 5611-5640.
3. A. C. Luntz and B. D. McCloskey, *Chem Rev*, 2014, **114**, 11721-11750.
4. X. Zhang, X. Wang, Z. Xie and Z. Zhou, *Green Energ Environ*, 2016, **1**, 4-17.
5. Y. Lu, H. A. Gasteiger, M. C. Parent, V. Chiloyan and Y. Shao-Horn, *Electrochem Solid-State Lett*, 2010, **13**, A69-A72.
6. B. D. McCloskey, A. Speidel, R. Scheffler, D. C. Miller, V. Viswanathan, J. S. Hummelshøj, J. K. Nørskov and A. C. Luntz, *J Phys Chem Lett*, 2012, **3**, 997-1001.
7. A. Débart, A. J. Paterson, J. Bao and P. G. Bruce, *Angew Chem Int Edit*, 2008, **47**, 4521-4524.
8. A. Débart, J. Bao, G. Armstrong and P. G. Bruce, *J Power Sources*, 2007, **174**, 1177-1182.
9. C. Sun, F. Li, C. Ma, Y. Wang, Y. Ren, W. Yang, Z. Ma, J. Li, Y. Chen, Y. Kim and L. Chen, *J Mater Chem A*, 2014, **2**, 7188-7196.
10. C. Ahn, R. S. Kalubarme, Y. Kim, K. Jung, K. Shin and C. Park, *Electrochim Acta*, 2014, **117**, 18-25.
11. H. Lim, H. Song, H. Gwon, K. Park, J. Kim, Y. Bae, H. Kim, S. Jung, T. Kim and Y. H. Kim, *Energ Environ Sci*, 2013, **6**, 3570-3575.
12. Y. Lu, Z. Xu, H. A. Gasteiger, S. Chen, K. Hamad-Schifferli and Y. Shao-Horn, *J Am Chem Soc*, 2010, **132**, 12170-12171.
13. Z. Peng, S. A. Freunberger, Y. Chen and P. G. Bruce, *Science*, 2012, **337**, 563-566.
14. H. Jung, Y. S. Jeong, J. Park, Y. Sun, B. Scrosati and Y. J. Lee, *ACS Nano*, 2013, **7**, 3532-3539.
15. M. M. Ottakam Thotiyl, S. A. Freunberger, Z. Peng and P. G. Bruce, *J Am Chem Soc*, 2013, **135**, 494-500.
16. X. Lin, L. Zhou, T. Huang and A. Yu, *Int J Electrochem Sc*, 2012, **7**, 9550-9559.
17. Y. Jiang, J. Cheng, L. Zou, X. Li, Y. Gong, B. Chi, J. Pu and J. Li, *Electrochim Acta*, 2016, **210**, 712-719.
18. L. Jia, X. Wang, W. Li, K. Li, B. Chi, J. Pu, L. Jian and S. Yuan, *J Power Sources*, 2014, **253**, 138-142.

19. L. Jia, K. Li, D. Yan, X. Wang, B. Chi, J. Pu, L. Jian and S. Yuan, *RSC Adv*, 2015, **5**, 7761-7765.
20. M. Nolan, S. C. Parker and G. W. Watson, *Phys Chem Chem Phys*, 2006, **8**, 216-218.
21. X. Wu, X. Gong and G. Lu, *Phys Chem Chem Phys*, 2015, **17**, 3544-3549.
22. J. Wang, M. Liu and M. C. Lin, *Solid State Ionics*, 2006, **177**, 939-947.
23. F. Chen, D. Liu, J. Zhang, P. Hu, X. Gong and G. Lu, *Phys Chem Chem Phys*, 2012, **14**, 16573-16580.
24. J. Zhu, X. Ren, J. Liu, W. Zhang and Z. Wen, *ACS Catal*, 2015, **5**, 73-81.
25. X. Zhang, X. Zhang, X. Wang, Z. Xie and Z. Zhou, *J Mater Chem A*, 2016, **4**, 9390-9393.
26. X. Ren, J. Zhu, F. Du, J. Liu and W. Zhang, *J Phys Chem C*, 2014, **118**, 22412-22418.
27. Z. Peng, Y. Chen, P. G. Bruce and Y. Xu, *Angew Chem Int Edit*, 2015, **54**, 8165-8168.
28. Y. Zhang, X. Zhang, J. Wang, W. C. McKee, Y. Xu and Z. Peng, *J Phys Chem C*, 2016, **120**, 3690-3698.
29. G. Yang, Y. Wang and Y. Ma, *The Journal of Physical Chemistry Letters*, 2014, **5**, 2516-2521.
30. C. M. Burke, V. Pande, A. Khetan, V. Viswanathan and B. D. McCloskey, *Proc Natl Acad Sci USA*, 2015, **112**, 9293-9298.
31. M. Baudin, K. Hermansson and N. V. Skorodumova, *Phys Rev B*, 2004, **69**, 75401.
32. J. Furthmüller and G. Kresse, *Phys Rev B*, 1996, **54**, 11169-11186.
33. K. Burke, M. Ernzerhof and J. P. Perdew, *Phys Rev Lett*, 1996, **77**, 3865-3868.
34. G. A. Botton, S. Y. Savrasov, C. J. Humphreys, A. P. Sutton and S. L. Dudarev, *Phys Rev B*, 1998, **57**, 1505-1509.
35. P. E. Blöchl, *Phys Rev B*, 1994, **50**, 17953-17979.
36. P. R. L. Keating, D. O. Scanlon, B. J. Morgan, N. M. Galea and G. W. Watson, *J Phys Chem C*, 2012, **116**, 2443-2452.
37. J. S. Hummelshøj, J. Blomqvist, S. Datta, T. Vegge, J. Rossmeisl, K. S. Thygesen, A. C. Luntz, K. W. Jacobsen and J. K. Nørskov, *J Chem Phys*, 2010, **132**, 71101.
38. Y. Jing and Z. Zhou, *ACS Catal*, 2015, **5**, 4309-4317.
39. T. A. Mellan, K. P. Maenetja, P. E. Ngoepe, S. M. Woodley, C. R. A. Catlow and R. Grau-Crespo, *J Mater Chem A*, 2013, **1**, 14879-14887.
40. F. Esch, S. Fabris, L. Zhou, T. Montini, C. Africh, P. Fornasiero, G. Comelli and R. Rosei, *Science*, 2005, **309**, 752-755.
41. J. L. F. Da Silva, J. Sauer and M. V. Ganduglia-Pirovano, *Phys Rev Lett*, 2009, **102**, 26101.
42. M. Reichling, A. Ishiyama, S. Morita, Ó. Custance and S. Torbrügge, *Phys Rev Lett*, 2007, **99**, 56101.
43. H. Wang, X. Gong, Y. Guo, Y. Guo, G. Lu, P. Hu and H. Li, *Phys Rev B*, 2009, **79**, 193401.
44. Y. M. Choi, H. Abernathy, H. T. Chen, M. C. Lin and M. Liu, *ChemPhysChem*, 2006, **7**, 1957-1963.
45. R. F. W. Bader, *Atoms in Molecules: A Quantum Theory*, Oxford University Press, 1990.
46. M. V. Ganduglia-Pirovano, J. Sauer, V. Bayer, G. Kresse and J. L. F. Da Silva, *Phys Rev B*, 2007, **75**, 45121.
47. J. Carrasco, K. M. Neyman, F. Illas and C. Loschen, *Phys Rev B*, 2007, **75**, 35115.
48. G. Girishkumar, B. McCloskey, A. C. Luntz, S. Swanson and W. Wilcke, *J Phys Chem Lett*, 2010, **1**, 2193-2203.
49. B. D. McCloskey, R. Scheffler, A. Speidel, D. S. Bethune, R. M. Shelby and A. C. Luntz, *J Am Chem Soc*, 2011, **133**, 18038-18041.
50. S. Nicola, *Nanotechnology*, 2009, **20**, 445703.
51. Y. Crespo and N. Seriani, *J Mater Chem A*, 2014, **2**, 16538-16546.
52. M. Lee, Y. Hwang, K. Yun and Y. Chung, *J Power Sources*, 2016, **307**, 379-384.
53. J. S. Hummelshøj, A. C. Luntz and J. K. Nørskov, *J Chem Phys*, 2013, **138**, 34703.

View Article Online
DOI: 10.1039/C6TA10233F

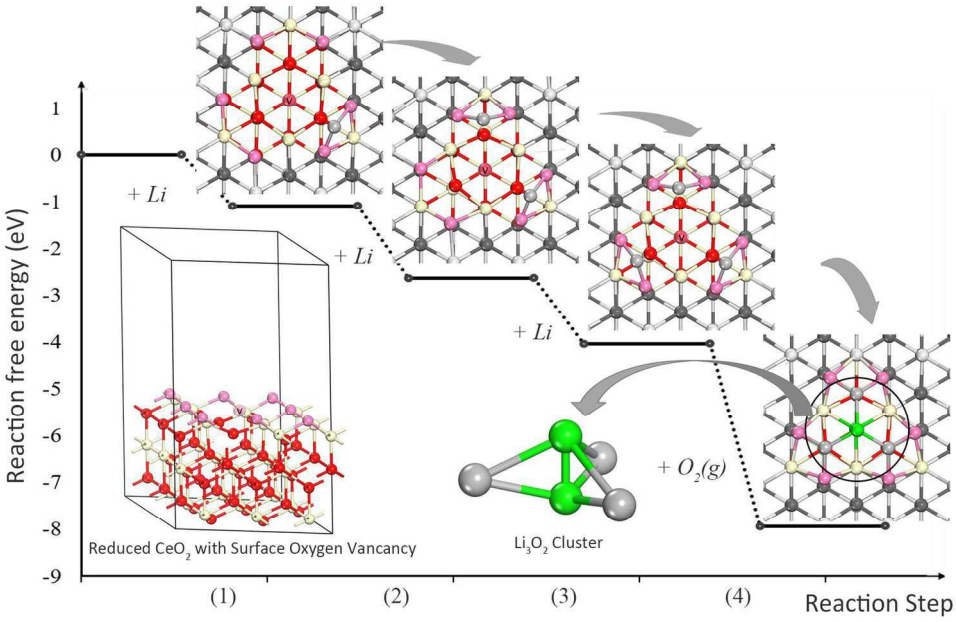

476x293mm (96 x 96 DPI)